HHS Public Access

Author manuscript

Magn Reson Med. Author manuscript; available in PMC 2024 September 01.

Published in final edited form as:

Magn Reson Med. 2023 September ; 90(3): 1053–1068. doi:10.1002/mrm.29700.

Live-View 4D GRASP MRI: A Framework for Robust Real-Time Respiratory Motion Tracking with A Sub-Second Imaging Latency

Li Feng

Center for Advanced Imaging Innovation and Research (CAI2R), New York University Grossman School of Medicine, New York, NY, United States

Biomedical Engineering and Imaging Institute and Department of Radiology, Icahn School of Medicine at Mount Sinai, New York, NY, United States

Abstract

Purpose: To propose a framework called live-view GRASP MRI for low-latency and high-fidelity real-time volumetric MRI.

Methods: Live-view GRASP MRI has two stages. The first one is called an off-view stage and the second one is called a live-view stage. In the off-view stage, 3D k-space data and 2D navigators are acquired alternatively using a new navi-stack-of-stars sampling scheme. A 4D motion database is then generated that contains time-resolved MR images at a sub-second temporal resolution, and each image is linked to a 2D navigator. In the live-view stage, only 2D navigators are acquired. At each time point, a live-view 2D navigator is matched to all the off-view 2D navigators. A 3D image that is linked to the best matched off-view 2D navigator is then selected for this time point. This framework places the typical acquisition and reconstruction burden of MRI in the off-view stage, enabling low-latency real-time 3D imaging in the live-view stage. The accuracy of live-view GRASP MRI and the robustness of 2D navigators for characterizing respiratory variations and/or body movements were assessed.

Results: Live-view GRASP MRI can efficiently generate real-time volumetric images that match well with the ground-truth references, with an imaging latency below 500ms. Compared to 1D navigators, 2D navigators enable more reliable characterization of respiratory variations and/or body movements that may occur throughout the two imaging stages.

Conclusion: Live-view GRASP MRI represents a novel, accurate and robust framework for real-time volumetric imaging, which can potentially be applied for motion adaptive radiotherapy on MRI-Linac.

Keywords

Live-view; GRASP; Real-time imaging; MRI-Linac; Navi-stack-of-stars; Respiratory motion

Address correspondence to: Li Feng, PhD, Center for Advanced Imaging Innovation and Research (CAI2R), New York University Grossman School of Medicine, 660 First Avenue, New York, NY, USA 10029, lifeng.mri@gmail.com.

Disclosure

Li Feng is a co-inventor of a patent on the GRASP and XD-GRASP MRI techniques and a patent on the MRSIGMA technique.

Introduction

In recent years, there has been a strong trend to use MRI for image-guided treatment beyond traditional diagnostic purposes (1–3). One example that has recently gained substantial interest is MRI-guided radiotherapy using an MRI-Linac system (4–7). Compared to image-guided radiotherapy based on computational tomography (e.g., cone-beam CT or CBCT), MRI provides superior soft-tissue contrast that enables better delineation of lesions and more precise tumor contouring (8–10). The synergy of MRI and Linac as a single modality also provides the feasibility of real-time motion adaptive radiotherapy, in which MR images can be acquired during treatment to guide adjustment of radiation beams according to organ changes (e.g., respiration-induced displacement) (11–14). This can help avoid excessive radiation delivery to surrounding healthy organs or tissues.

Two essential requirements for MRI-guided adaptive radiotherapy are (a) a low imaging latency, which can be simply approximated as the sum of data acquisition and image reconstruction time, and (b) high imaging fidelity that ensures robustness to variations of respiratory patterns, body movements and other unwanted effects (15). For the first requirement, a latency below 500 milliseconds (ms) has been recommended to account for respiratory motion in MRI-guided radiotherapy (15,16). Unfortunately, the imaging speed of MRI is insufficient to meet this requirement. For example, 500ms might be barely enough to acquire and reconstruct a 2D MR image with a coarse spatial resolution. Given these considerations, clinical MRI-Linac systems often use 2D cine imaging for motion tracking, although 3D cine imaging is highly desired. To meet the requirement of imaging fidelity, MRI techniques implemented on an MRI-Linac scanner should be robust against various motion uncertainties, such as respiratory drifts, irregular breathing, or patient movements.

Over the past decade, various 4D (3D+time) MRI methods have been proposed for treatment planning in radiotherapy (17–25). These methods typically employ advanced reconstruction techniques, such as compressed sensing and/or low-rank algorithms, to generate dynamic volumetric images. However, standard 4D MRI techniques exploiting spatiotemporal correlations are difficult for motion adaptive radiotherapy, as they require all dynamic data to be acquired before retrospective image reconstruction can start, thus leading to a long imaging latency. The advent of deep learning has provided a promising solution to help reduce both acquisition and reconstruction time in general (26–28), but it remains to be explored whether deep learning alone can achieve a sub-second imaging latency for high-fidelity volumetric imaging.

A more practical solution to address these challenges towards real-time motion adaptive radiotherapy could be a two-stage imaging approach. The first stage, referred to as “off-view” in this work, is performed as a preparation step while the radiation beam is turned off with the patient in place on the MRI-Linac scanner. The purpose of this stage is to acquire and reconstruct a 4D motion database (slow) that contains 3D MR images corresponding to distinct motion phases, with each motion phase linked to a navigator (a signature) acquired with the image data. The second stage, referred to as “live-view” in this work, is performed during adaptive treatment while the radiation beam can be turned on, and it acquires

navigators only (fast). At this stage, a newly acquired navigator is compared or matched to all the navigators acquired in the off-view stage, and a 3D image in the 4D motion database linked to the best-matched off-view navigator is then selected for the current time point in the live-view stage. This two-stage imaging strategy shifts the lengthy data acquisition and image reconstruction process to the first off-view stage, leaving navigator-only acquisition and a simple matching process (referred to as nav-matching hereafter) for the second live-view stage to enable real-time low-latency 3D MRI. In this two-stage framework, navigators are specifically referred to the data used for nav-matching, and a navigator can have different dimensionality as described below.

MRSIGMA (MR SIGnature MAtching) was one of the first approaches to demonstrate this idea (29). In MRSIGMA, a respiratory-resolved 4D motion database is generated using XD-GRASP (eXtral-Dimensional Golden-angle RAdial Sparse Parallel imaging). Radial k-space data is binned into different respiratory phases based on a motion signal extracted from k-space centers (23). This motion signal also serves as the navigators for nav-matching. However, MRSIGMA suffers from several major limitations that can restrict its practical performance. First, although MRSIGMA used 1D projections (formed from the centers of radial k-space) to generate a motion signal, only one data point from the motion signal was used for nav-matching at each time. Therefore, MRSIGMA is essentially a 0D-navigator approach, as each navigator only contains one data point that provides limited information for nav-matching. Moreover, data from k-space centers may be sensitive to MRI scanner errors (e.g., gradient delay). Second, MRSIGMA requires an explicit motion detection process for data binning and generation of 0D navigators, which may need user interaction for refinement. Third, MRSIGMA relies on an assumption of uniform and stable breathing, since it requires motion sorting to generate respiratory-resolved 4D images in the off-view stage. Any motion drifts, respiratory variations or body movements can cause image blurring in the motion database. Fourth, MRSIGMA generates limited motion phases (e.g., 10 motion images as described in (29)), which may not be sufficient to fully characterize respiratory variation. Fifth, 0D navigators contain limited information and may not be reliable for detecting respiratory variations and/or patient movements that can occur within the off-view stage or between the two stages, which is a major challenge that any two-stage method should address.

Another technique that adopted the idea of two-stage imaging is single projection driven real-time MR imaging (SPIDERM) (30). Instead of generating a respiratory-resolved motion database, SPIDERM aims to reconstruct a spatial basis that serves as a motion database to generate real-time 3D images. External head-to-foot 1D projections are periodically acquired throughout the two stages as navigators. Thus, SPIDERM is a 1D-navigator approach that can be more reliable than MRSIGMA. However, 1D navigators may not be able to accurately characterize different types of respiratory variations that may occur within the off-view stage or between the two stages. Meanwhile, acquisition of head-to-foot 1D navigators requires rapid switching of gradients, which may introduce eddy-current artifacts.

The purpose of this work was to propose and demonstrate a new framework called live-view GRASP (Golden-angle RAdial Sparse Parallel) MRI as a novel extension to optimize the two-stage imaging scheme based on GRASP reconstruction. Compared to prior two-stage

methods, live-view GRASP provides several unique features, including (a) reconstruction of time-resolved high-temporal-resolution 4D images as a motion database, (b) elimination of the need for explicit motion detection and data sorting, and (c) use of 2D navigators for 2D nav-matching and more accurate motion characterization.

Methods

The Live-View GRASP MRI Framework

This section first defines terminology that will be used in this work and summarizes key components of live-view GRASP MRI. As shown in Figure 1, the first stage is called an off-view stage, which aims to generate a time-resolved 4D motion database. Each off-view 3D image in the motion database is linked to a 2D navigator that is referred to as an off-view navigator. The second stage is called a live-view stage, which only acquires 2D navigators that are referred to as live-view navigators. Live-view GRASP MRI includes three novel components, including (a) a new sampling scheme called navi-stack-of-stars to jointly acquire 3D imaging data and corresponding off-view 2D navigators (for the off-view stage), (b) Low-rank subspace-based MRI reconstruction (31,32) to generate time-resolved 4D images with a sub-second temporal resolution (for the off-view stage), and (c) 2D nav-matching to efficiently generate 3D images in real time (referred to as live-view 3D images) with a low latency in the live-view stage. Details about these components are described below.

3D Navi-Stack-of-Stars Sampling—The proposed navi-stack-of-stars sampling scheme is shown in Figure 2. Here, k-space lines from different slice locations at a given rotation angle is called a radial stack. A partition-in-line sampling loop, as described in (33), is implemented. Compared to standard golden-angle stack-of-stars sampling that acquires radial stacks continuously rotated by a golden angle (Figure 2a), navi-stack-of-stars sampling (Figure 2b) alternatively acquires both regular radial stacks rotated by a golden angle and navigator stacks all with a 0-degree acquisition angle. The navigator stacks are acquired with same imaging parameters (e.g., number of slices, TR/TE and slice reordering) as for acquiring regular stacks without affecting imaging steady state. In our current implementation, a navigator stack is acquired following every two regular radial stacks to achieve a high temporal resolution. The navi-stack-of-stars sampling is employed for the off-view stage, where the 0-degree navigator stacks become off-view 2D navigators after a 2D FFT followed by multicoil combination using sum of square.

4D Golden-Angle MRI Reconstruction—From the acquired navi-stack-of-stars data, time-resolved 4D images with a sub-second temporal resolution are reconstructed to generate a 4D motion database. Image reconstruction is done using GRASP-Pro – a technique that was recently developed for highly-accelerated 4D MRI (31,32). Different from XD-GRASP that relies on explicit respiratory motion detection and data binning to reduce motion blurring, GRASP-Pro implicitly achieves this by reconstructing dynamic images at a temporal resolution that is high enough to resolve respiratory motion (32). Accordingly, GRASP-Pro is expected to be more robust than XD-GRASP, as shown in (32). In this work, GRASP-Pro reconstructs a 3D image volume from two regular radial stacks (2

radial spokes in each slice), as shown in Figure 2b. In this way, each 3D image volume is uniquely linked to an off-view 2D navigator acquired between the two regular stacks. Details about GRASP-Pro implementation are provided in Supporting Information Materials.

2D Nav-Matching—In live-view GRASP MRI, nav-matching is performed based on 2D pattern matching between the off-view and live-view 2D navigators, as illustrated in Figure 1. At each time point in the live-view stage, a 2D live-view navigator is acquired and is compared to all the 2D off-view navigators. A 3D image linked to the off-view navigator that best matches the newly acquired live-view navigator is selected as the 3D image for the current time point. The matching is performed based on the structure similarity index (SSIM), and a threshold of 0.8 is empirically set to determine whether the matching is acceptable. A SSIM value below 0.8 indicates a potential variation of respiratory pattern (due to, for example, deep breathing) between the current live-view navigator and the motion database. In this case, the radiation beam can be turned off to stop treatment for this time point in practical implementation. If the SSIM values are consistently low, that may imply changes of patient position (e.g., due to body movements or motion drifts). In this case, the off-view stage could be repeated. This two-stage imaging approach enables efficient generation of 3D images in the live-view stage without lengthy acquisition and reconstruction. At each time point, the total imaging latency only includes time to acquire a 2D live-view navigator, time to perform a 2D FFT, time to calculate the SSIM for 2D nav-matching, and time to fetch a 3D image from the motion database. These steps are highly parallelizable, so that the total imaging latency can be reduced to 500ms or below as recommended (15,16).

Imaging Experiments

Overall Experimental Design—Under a good breathing condition (e.g., regular breathing without body movements), different types of navigators (0D, 1D or 2D) are expected to achieve similar performance in two-stage imaging (28,29). However, in practice, breathing patterns in clinical patients can be complex and hard to predict, and this can be further exacerbated when body movements occur. Therefore, timely detection of breathing pattern variations or potential body movements is essential for any two-stage imaging method implemented for motion adaptive radiotherapy. Given these considerations, 2D navigators are expected to be more reliable than 1D or 0D navigators for detecting motion drifts and/or body movements that may occur in the off-view stage and for detecting inconsistencies between the off-view stage and the live-view stage (e.g., due to patient movements between the two stages). Under these unwanted conditions, treatment can be paused, and the off-view stage can be repeated.

To validate these hypotheses, four in-vivo imaging experiments, as summarized below, have been designed to demonstrate the performance and robustness of live-view GRASP MRI. In addition, the improvement of time-resolved GRASP-Pro reconstruction over respiratory-resolved XD-GRASP reconstruction for generating a 4D motion database was also demonstrated.

- Experiment 1: To assess the performance of 2D navigators for characterizing respiratory variations and/or body movements in the off-view stage. This was performed in two sub-studies under different breathing conditions.
- Experiment 2: To validate the accuracy of live-view GRASP MRI with 2D navigator-based nav-matching.
- Experiment 3: To assess the performance of 2D navigators for detecting body movements that may occur between the off-view and live-view stages.
- Experiment 4: To demonstrate the feasibility of navigator-only live-view scans in live-view GRASP MRI.

All in-vivo studies were performed on a 3T MRI scanner (Magnetom Skyra, Siemens Healthcare AG, Erlangen, Germany) using a fat-saturated 3D radial sequence with navi-stack-of-stars sampling. Human imaging experiments were HIPAA-compliant and were approved by the Institutional Review Board (IRB). Written informed consent was obtained from all subjects. Imaging was performed on the upper abdomen of all subjects. All image reconstruction tasks were implemented in an NVIDIA DGX-1 server.

Experiment 1—The first experiment was designed to assess the performance of 2D navigators for characterizing respiratory variations and/or body movements in the off-view stage. For this purpose, only off-view scans were performed. Specifically, two imaging studies were performed in this experiment under two different conditions. For the first study, off-view scans were performed on a total of 24 subjects (age=45±17 years, 19 males and 5 females), including 17 healthy volunteers and 7 patients with hepatocellular carcinoma (HCC). A total of 24 off-view datasets were acquired for this study. No breathing instructions were given for any of the scans, so that the subjects could breathe in any way they wanted. For the second study, off-view scans were performed on 9 healthy volunteers (age= 32±5 years, 6 males and 3 females). All subjects were asked to move their body once during the scan in any way they wanted. This process was repeated, with the subjects asked to move their body once more in a different way. As a result, a total of 18 off-view datasets were acquired for this study.

Relevant imaging parameters for all data acquisitions included: FOV=360×360mm^2, matrix size=256×256, spatial resolution=1.4×1.4mm^2, slice thickness=5mm, number of slices=40, slice partial Fourier=75%, TR/TE=2.75/1.21ms, flip angle=10°. Slab-selective excitation was employed. A total of 1500 radial stacks, including 1000 golden-angle rotated stacks and 500 navigator stacks (angle=0°) were acquired. The total acquisition time was 2:49 min. For image reconstruction, the first 31 radial stacks were discarded since data in the beginning were not acquired in a full steady state. This led to 489 2D navigators [(1500-31)/3] and corresponding 489 3D images with every two radial stacks reconstructed as a 3D image volume. The temporal resolution of the resulting 4D MR images was ~0.3s/volume. The acquisition protocol and reconstruction scheme were also used in other experiments below.

For image analysis, the SSIM between the last 3D image and all the previous 3D images was calculated for each subject, which generated 488 SSIM values. The SSIM values constitute a signal curve (referred to as the SSIM curve hereafter) that reflects underlying

motion variations. This served as a ground-truth reference since it was obtained from 3D images. Next, the same SSIM curves were calculated using both 2D and 1D navigators for comparison. 1D navigators were obtained by taking the *kz*-directional central k-space lines from the 0° navigator stacks followed by a 1D FFT and multicoil combination using sum of square, as shown in the Supporting Information Materials. Correlation coefficients (CCs) between the SSIM curves obtained from reference 3D images and either 2D or 1D navigators were calculated, and their differences were assessed using the Wilcoxon signed-rank test. The hypothesis of this experiment was that 2D navigators enable more accurate characterization of respiratory variations than 1D navigators. Here, a higher CC indicates a higher positive correlation with the reference and thus better performance. Generally, a CC above 0.9 indicates a very high positive correlation (34).

Experiment 2—Experiment 2 was performed on the same 9 volunteers from the previous experiment. For each subject, two identical data acquisitions were performed using the navi-stack-of-stars sequence. The first scan represented the off-view stage and the second scan represented the live-view stage. A 10-minute gap was placed between the two scans to emulate a delay that is needed in practical implementation of the two-stage framework for different tasks, such as 4D MRI reconstruction and tumor contouring. In this experiment, imaging data were also acquired for the live-view scan for the purpose of generating ground-truth 3D images for comparison, as described in Supporting Information Materials for more details. It should be noted that in practice, acquisition of imaging data is not needed in the live-view stage. All subjects were asked to stay still and breathe normally during the scans and the gap to achieve a good breathing condition. Here, 3D images reconstructed from the live-view scan were treated as ground-truth references for validating 2D nav-matching.

For data analysis, 50 consecutive live-view 2D navigators were selected from each subject, and the corresponding 50 live-view 3D images were generated with 2D nav-matching. These nav-matched live-view 3D images were then compared to the corresponding reference 3D images by calculating the SSIM. For additional comparison, nav-matching was also performed using 1D navigators. The Wilcoxon signed-rank test was used to compare the SSIM values obtained with 2D nav-matching and 1D nav-matching. Here, a higher SSIM indicates better accuracy of nav-matching. Another purpose of this experiment was also to obtain the (maximum) SSIM values that were used for nav-matching across different data points and different subjects under a good breathing condition, and this serves as a baseline SSIM for comparison in experiment 3.

Experiment 3—This experiment was designed to assess the performance of 2D navigators for detecting body movements that may occur between the off-view and live-view stages. Imaging studies were performed on the 9 volunteers as before. For each subject, two identical data acquisitions were performed using the 3D navi-stack-of-stars sequence to acquire both imaging and navigator data. The first scan represented the off-view stage and the second scan represented the live-view stage. The subjects were asked to relax and move (in any way they wanted) between the scans. As a result, the off-view and the live-view scans were expected to be performed at different body positions.

For data analysis, a 2D live-view navigator was randomly selected from each subject, and the SSIM between this navigator and all the off-view 2D navigators from this subject were calculated. This process was repeated for 1D live-view navigators at the same time point for comparison. In addition, since the live-view scans were performed using the navi-stack-of-stars sequence, ground-truth reference 3D images were available (see Supporting Information Materials), and the SSIM between the reference 3D image at this time point with all the off-view 3D images were calculated as a ground truth for comparison. The hypothesis of this experiment was that when body movements occur between the off-view and the live-view stages, SSIM values obtained between a live-view navigators with off-view navigators should be lower than the baseline SSIM obtained from experiment 2. A larger deviation from the baseline SSIM indicates that a method can more reliably identify the movements, while a smaller deviation indicate that a method may not be able to identify the movements correctly.

Experiment 4—In practice, a live-view scan is expected to acquire navigators only. Thus, experiment 4 was designed to demonstrate the feasibility of navigator-only live-view scans. In this experiment, two data acquisitions were performed on the same 9 volunteers. The off-view scan was performed as above, while the live-view scan acquired 100 2D navigators continuously without acquiring imaging data (only 0° navigator stacks). A 10-minute gap was placed between the two scans, and all subjects were asked to stay still and breathe normally during the scans and the gap. For each subject, 100 live-view 3D images were generated from corresponding live-view navigators with 2D nav-matching.

For data analysis, the SSIM between the last live-view 3D image and all the previous 3D images was calculated to represent a motion variation pattern consisting of 99 SSIM values. Due to lack of ground-truth references, the SSIM between the last live-view 2D navigator with all the previous 2D navigators was calculated, and the resulting SSIM curve served as a reference for comparison. For each subject, a correlation coefficient (CC) was calculated between the SSIM curves calculated from the live-view 3D images and the live-view 2D navigators. The hypothesis of this experiment was that motion variation patterns obtained from the live-view 3D images can match well with that from the live-view 2D navigators. A CC above 0.9 generally indicates a very high positive correlation (34).

Results

Imaging Latency

All experiments were successfully conducted. Live-view GRASP MRI with a navigator-only live-view scan was able to achieve a total imaging latency as recommended in (16). With a standard implementation in MATLAB, the estimated total imaging latency for generating each live-view 3D image was between 0.4–0.5s, including time to acquire a 0° navigator stack (~0.11s), time to perform a 2D FFT on the navigator stack for generating a 2D navigator (~0.015s), time to perform 2D nav-matching (~0.25–0.3s with parallel computing), and time to fetch a 3D image from the motion database (0.005–0.01s). The average time for 4D MRI reconstruction in the off-view stage was 58.35±3.95 min.

Respiratory-Resolved Reconstruction vs Time-Resolved Reconstruction

The advantage of GRASP-Pro reconstruction over XD-GRASP reconstruction has been previously demonstrated (32), and it is further demonstrated in Figure 3. Here, XD-GRASP reconstruction was performed with 10 respiratory phases as implemented in (29). Motion sorting in XD-GRASP reconstruction was performed using a respiratory signal extracted from k-space central projections, as described before (23,35). Results in Figure 3a are from a patient with HCC imaged during irregular breathing. GRASP-Pro reconstruction was able to resolve respiratory motion with a temporal resolution of ~0.3s/volume, while XD-GRASP suffers from residual motion blurring, particularly in the HCCs (yellow arrows). Results in Figure 3b are from a volunteer imaged with body movement during the scan, which is highlighted in the projections with a green arrow. The movement, however, cannot be captured in the extracted respiratory signal and it led to blurring in respiratory-resolved XD-GRASP images. In contrast, time-resolved GRASP-Pro reconstruction yielded better image quality. These results suggest that GRASP-Pro is a superior and more robust method for generating a 4D motion database.

Experiment 1

Experiment 1 evaluated the performance of live-view GRASP MRI for detecting respiratory variations and/or body movements in the off-view stage. Figure 4 shows SSIM curves from two representative subjects from study 1 (without prescribed breathing instruction during scans) comparing the performance for detecting respiratory variations using 2D and 1D navigators. Although both navigators could detect irregular breathing in the first subject, 1D navigators failed to detect a motion drift in the second subject. In contrast, 2D navigators were able to detect the drift, which was also seen in the reference 3D images. Corresponding cine movies from these two subjects are shown in Supporting Information Video 1 and Video 2.

Figure 5 shows the same SSIM curves from two representative subjects from study 2 (with prescribed body movement during the scans) comparing the performance for detecting respiratory variations using 2D and 1D navigators. The first subject had an obvious body movement while the second subject only had a small movement, as indicated in the reference 3D images. For both subjects, the body movement was not captured by 1D navigators but was successfully detected by 2D navigators. Corresponding cine movies from these two subjects (4 different slices) are shown in Supporting Information Video 3 and Video 4.

Figure 6 plots the correlation coefficients (CCs) for all the 24 datasets from study 1 (left) and all the 18 datasets from study 2 (right) that compare the SSIM curves between 3D reference images and 2D or 1D navigators. The results indicate that 2D navigators are superior for detecting respiratory variations and/or body movements in the off-view stage compared to 1D navigators. Statistically, the CCs were 0.886 ± 0.049 between 2D navigators and the reference and were 0.791 ± 0.148 between 1D navigators and the reference (P=2.07e-05, n=24) for study 1. The CCs were 0.967 ± 0.023 between 2D navigators and the reference and were 0.721 ± 0.244 between 1D navigators and the reference (P=2.33e-04, n=18) for study 2.

Experiment 2

Experiment 2 validated the accuracy of live-view GRASP MRI and compared 2D nav-matching and 1D nav-matching under a good breathing condition. Figure 7 shows two live-view 2D navigators and corresponding live-view 3D images from one subject at two different time points. The live-view 3D images visually match well with the reference 3D images. Corresponding cine movies from this subject are shown in Supporting Information Video 5.

Figure 8a compares live-view 3D images obtained with 2D nav-matching and 1D nav-matching along with corresponding reference 3D images in another subject. Figure 8b shows SSIM values that were calculated between reference 3D images and live-view 3D images with 2D nav-matching (left) and SSIM values between reference 3D images and live-view 3D images with 1D nav-matching (right). The results were obtained from a total of 450 time points (9 subjects and 50 time points each). There were no significant differences in 8 subjects ($P=0.074–0.46$) between 2D nav-matching and 1D nav-matching, while 2D nav-matching was better ($P=0.0039$) only in one subject. The results have suggested that when a subject can stay still and breathe consistently, both 2D and 1D nav-matching can generate accurate live-view 3D images. The (maximum) SSIM values obtained for nav-matching were 0.934 ± 0.047 for 1D navigators and 0.881 ± 0.044 for 2D navigators averaged over all the data points and all the subjects. Corresponding SSIM values between the live-view 3D images and the reference 3D images were 0.875 ± 0.033. These values are treated as a baseline when nav-matching is performed under a good breathing condition without body movements.

Experiment 3

Experiment 3 compared the performance of 2D and 1D navigators for detecting body movements that may occur between the off-view and live-view stages. Results from two representative subjects are shown in Figure 9. In the first subject (left), there is a clear shift of body position between the off-view stage and the live-view stage (yellow arrows). The SSIM values obtained from both 3D images and 2D navigators are consistently low, indicating detection of the body movement, while the SSIM values obtained from 1D navigators are higher, suggesting that 1D navigators cannot characterize the body movement well. A similar finding was observed in the second subject (right). For this subject, the shift of body position was very small as indicated by the red arrows in the 3D images. The difference of body position could be identified from both 3D images and 2D navigators with consistently low SSIM values, while the SSIM values obtained from 1D navigators are higher. Summarizing results from all the 9 subjects, the maximum SSIM values between live-view and off-view navigators were 0.832 ± 0.123 for 1D navigator and were 0.484 ± 0.156 for 2D navigator. Corresponding SSIM values between the live-view 3D images and the reference 3D images were 0.689 ± 0.061. Compared to the baseline SSIM obtained in experiment 2, it can be seen that when body movements occur, 2D navigator-based nav-matching leads to a 45% reduction in SSIM while 1D navigator-based nav-matching only leads to 11% of reduction in SSIM. Note that in this experiment, a large deviation of the maximum SSIM from the baseline value indicates better performance in detecting the change of body position occurring between the off-view and live-view stages.

Experiment 4

Experiment 4 demonstrated the performance of live-view GRASP MRI when a live-view scan only acquires 2D navigators. Figure 10a shows live-view 2D navigators and resulting live-view 3D images at two different time points from a subject. SSIM curves calculated from the 3D images (red curve) and the 2D navigators (blue curve) are shown in Figure 10b with a strong correlation (CC=0.9344). Corresponding cine movies from this subject are shown in Supporting Information Video 6. For all the 9 subjects, the CCs between the live-view 3D images and 2D navigators were 0.924 ± 0.051. The results have demonstrated the feasibility of live-view GRASP MRI with navigator-only live-view scanning, which is a situation one would expect in practice.

Discussion

This work proposed a framework called live-view GRASP MRI to enable low-latency and high-fidelity real-time 3D imaging, which could potentially be applied for motion adaptive radiotherapy on an MRI-Linac system. The proposed imaging framework includes two imaging stages. The off-view stage generates a 4D motion database with associated 2D navigators. The live-view stage can only acquire 2D navigators, and real-time 3D images can be efficiently generated with simple 2D pattern matching using acquired navigators.

Although the idea of two-stage imaging was previously explored in MRSIGMA (29) and SPIDERM (30), there are a number of limitations in these two approaches. A major limitation of MRSIGMA, among several others, is the generation of a motion database based on respiratory-resolved 4D imaging, which requires an explicit step for motion extraction and relies on stable and uniform breathing. In addition, the use of 0D navigators for nav-matching in MRSIGMA can be limited in characterizing different motion uncertainties. Although the use of 1D navigators in SPIDERM improves this situation, 1D navigators are still not sufficient to detect some types of movements that may occur in practice, as shown in this work. Moreover, SPIDERM uses a pre-learned spatial basis to generate 3D images in real time. This relies on matrix multiplication, which could be computationally expensive with higher dimensional navigators.

Live-view GRASP MRI proposes several components to address these limitations. First, a new sampling scheme called navi-stack-of-stars has been developed for the off-view stage, which embeds 2D navigators periodically into stack-of-stars golden-angle radial sampling. The main advantage of using 2D navigators over 0D or 1D navigators is the ability to characterize and identify unexpected respiratory variations and/or body movements within the off-view stage and/or between the two stages, as demonstrated in the above experiments. This is expected to be a very important feature, as a consistent breathing condition may not always be available, and therefore, the ability to characterize respiratory variations and/or body movements using navigators is highly important and necessary. Once a good breathing condition is obtained, live-view GRASP MRI is able to generate real-time live-view 3D images efficiently. Second, the motion database in live-view GRASP MRI consists of time-resolved 4D images without the need for explicit motion detection. In this work, a temporal resolution of ~0.3s/volume was obtained, which is sufficient to resolve respiratory

motion. Third, when 2D navigators are used, nav-matching could be efficient with parallel computing to ensure a low imaging latency.

Another major advantage of using 2D navigators is practical implementation of navigator-only live-view scans, as demonstrated in this work. To date, navigator-only live-view scans have not been demonstrated in both MRSIGMA and SPIDERM. One reason behind this could be the need to maintain consistence of navigator acquisition between two imaging stages. For example, although MRSIGMA only needs 0D navigators, full radial stacks are still acquired in its live-view stage (29), since they are needed to extract a motion signal in a similar way as that in the off-view stage. Similarly, SPIDERM acquires both head-to-foot 1D navigators and stack-of-stars imaging data alternatively in both off-view and live-view stages. This acquisition scheme requires rapid and large gradient changes to alternatively acquire image data and 1D navigators, which may introduce eddy currents to the 1D navigators. If only 1D navigators are acquired in the live-view stage, there will be minimum eddy currents, and thus the 1D live-view navigators may not match well with the off-view navigators acquired with lager gradient jumps. This could be a restriction of using 0D or 1D navigators for the live-view stage in practice.

A major limitation of live-view GRASP MRI, with its current implementation, is the slow reconstruction speed to generate a 4D motion database. This is attributed to two reasons. First, our proof-of-concept implementation has been implemented in MATLAB. Second, a large number of 3D images need to be reconstructed for the 4D motion database. However, it is expected that this challenge could be addressed with deep learning-based image reconstruction in high-performance GPU servers (26–28), which could substantially reduce waiting time between the off-view and live-view stages. Meanwhile, it is also possible that there is no need to generate so many 3D images for the motion database, but this will require additional investigation in future work.

This study also has a few other limitations that need discussion. First, this study used a gradient echo (GRE) sequence on a 3T scanner for proof of concept. However, 3T MRI-Linac systems are not available to date. Although the SNR of a GRE sequence becomes lower at lower magnetic field, it is expected that other sequences, such as balanced steady-state free precession (bSSFP) sequence, can be more reliably implemented, which enables good SNR and contrast. The selection and optimization of imaging sequence are certainly another important topic that requires careful investigation in future work. Another limitation of live-view GRASP MRI is the need to store a large number of 3D images for a 4D motion database. This may require a large amount of memory. Therefore, it is important to study whether a smaller number of 3D images would be sufficient to ensure good 4D MRI reconstruction and 2D nav-matching.

Conclusion

This study has proposed a new framework called live-view GRASP MRI. It represents a novel, accurate and robust framework to extend the two-stage imaging scheme for low-latency and high-fidelity real-time volumetric imaging. The primary application of live-view GRASP MRI will be adaptive radiotherapy on an MRI-Linac system.

Supplementary Material

Refer to Web version on PubMed Central for supplementary material.

Acknowledgement

This work was supported in part by the NIH (R01EB030549, R01EB031083, R21EB032917). The author thanks Dr. Tobias Block for sharing the stack-of-stars sequence to develop the navi-stack-stars sampling scheme and Ding Xia for supporting sequence implementation. The author also thanks Sera Saju for supporting enrollment of volunteers and patients and thanks Dr. Philip Robson for help edit the paper.

References

1. Mittauer K, Paliwal B, Hill P, et al. A New Era of Image Guidance with Magnetic Resonance-guided Radiation Therapy for Abdominal and Thoracic Malignancies. Cureus 2018;10 doi: 10.7759/CUREUS.2422.
2. Corradini S, Alongi F, Andratschke N, et al. MR-guidance in clinical reality: current treatment challenges and future perspectives. Radiat. Oncol. 2019 141 2019;14:1–12 doi: 10.1186/S13014-019-1308-Y.
3. Pollard JM, Wen Z, Sadagopan R, Wang J, Ibbott GS. The future of image-guided radiotherapy will be MR guided. Br. J. Radiol. 2017;90 doi: 10.1259/BJR.20160667.
4. Hall WA, Paulson ES, van der Heide UA, et al. The transformation of radiation oncology using real-time magnetic resonance guidance: A review. Eur. J. Cancer 2019;122:42–52 doi: 10.1016/J.EJCA.2019.07.021. [PubMed: 31614288]
5. Yuan J, Poon DMC, Lo G, Wong OL, Cheung KY, Yu SK. A narrative review of MRI acquisition for MR-guided-radiotherapy in prostate cancer. Quant. Imaging Med. Surg. 2022;12:1585 doi: 10.21037/QIMS-21-697. [PubMed: 35111651]
6. Raaymakers BW, Jürgenliemk-Schulz IM, Bol GH, et al. First patients treated with a 1.5 T MRI-Linac: clinical proof of concept of a high-precision, high-field MRI guided radiotherapy treatment. Phys. Med. Biol. 2017;62:L41 doi: 10.1088/1361-6560/AA9517. [PubMed: 29135471]
7. Lagendijk JJW, Raaymakers BW, Raaijmakers AJE, et al. MRI/linac integration. Radiother. Oncol. 2008;86:25–29 doi: 10.1016/J.RADONC.2007.10.034. [PubMed: 18023488]
8. Chandarana H, Wang H, Tijssen RHN, Das IJ. Emerging role of MRI in radiation therapy. J. Magn. Reson. Imaging 2018;48:1468–1478 doi: 10.1002/JMRI.26271. [PubMed: 30194794]
9. Gurney-Champion OJ, Versteijne E, van der Horst A, et al. Addition of MRI for CT-based pancreatic tumor delineation: a feasibility study. Acta Oncol. 2017;56:923–930 doi: 10.1080/0284186X.2017.1304654. [PubMed: 28375667]
10. Glide-Hurst CK, Paulson ES, McGee K, et al. Task group 284 report: magnetic resonance imaging simulation in radiotherapy: considerations for clinical implementation, optimization, and quality assurance. Med. Phys. 2021;48:e636–e670 doi: 10.1002/MP.14695. [PubMed: 33386620]
11. Nijkamp J, Pos FJ, Nuver TT, et al. Adaptive Radiotherapy for Prostate Cancer Using Kilovoltage Cone-Beam Computed Tomography: First Clinical Results. Int. J. Radiat. Oncol. Biol. Phys. 2008;70:75–82 doi: 10.1016/j.ijrobp.2007.05.046. [PubMed: 17869445]
12. Otazo R, Lambin P, Pignol JP, et al. MRI-guided Radiation Therapy: An Emerging Paradigm in Adaptive Radiation Oncology. Radiology 2021;298:248–260 doi: 10.1148/RADIOL.2020202747/ASSET/IMAGES/LARGE/RADIOL.2020202747.FIG9.JPEG. [PubMed: 33350894]
13. Hunt A, Hansen VN, Oelfke U, Nill S, Hafeez S. Adaptive Radiotherapy Enabled by MRI Guidance. Clin. Oncol. (R. Coll. Radiol). 2018;30:711–719 doi: 10.1016/J.CLON.2018.08.001. [PubMed: 30201276]
14. Tran EH, Eiben B, Wetscherek A, et al. Evaluation of MRI-derived surrogate signals to model respiratory motion. Biomed. Phys. Eng. Express 2020;6:045015 doi: 10.1088/2057-1976/AB944C. [PubMed: 33194224]

15. Goodburn RJ, P Philippens ME, Lefebvre TL, et al. The future of MRI in radiation therapy: Challenges and opportunities for the MR community. Magn. Reson. Med. 2022;88:2592–2608 doi: 10.1002/MRM.29450. [PubMed: 36128894]
16. Keall PJ, Mageras GS, Balter JM, et al. The management of respiratory motion in radiation oncology report of AAPM Task Group 76. Med. Phys. 2006;33:3874–3900 doi: 10.1118/1.2349696. [PubMed: 17089851]
17. Stemkens B, Paulson ES, Tijssen RHN. Nuts and bolts of 4D-MRI for radiotherapy. Phys. Med. Biol. 2018;63 doi: 10.1088/1361-6560/AAE56D.
18. Freedman JN, Collins DJ, Gurney-Champion OJ, et al. Super-resolution T2-weighted 4D MRI for image guided radiotherapy. Radiother. Oncol. 2018;129:486–493 doi: 10.1016/J.RADONC.2018.05.015. [PubMed: 29871813]
19. Johansson A, Balter JM, Cao Y. Gastrointestinal 4D MRI with respiratory motion correction. Med. Phys. 2021;48:2521–2527 doi: 10.1002/MP.14786. [PubMed: 33595909]
20. Nie X, Saleh Z, Kadbi M, et al. A super-resolution framework for the reconstruction of T2-weighted (T2w) time-resolved (TR) 4DMRI using T1w TR-4DMRI as the guidance. Med. Phys. 2020;47:3091–3102 doi: 10.1002/MP.14136. [PubMed: 32166757]
21. Li G, Wei J, Kadbi M, et al. Novel Super-Resolution Approach to Time-Resolved Volumetric 4-Dimensional Magnetic Resonance Imaging With High Spatiotemporal Resolution for Multi-Breathing Cycle Motion Assessment. Int. J. Radiat. Oncol. Biol. Phys. 2017;98:454–462 doi: 10.1016/J.IJROBP.2017.02.016. [PubMed: 28463165]
22. Mickevicius NJ, Paulson ES. On the use of low-dimensional temporal subspace constraints to reduce reconstruction time and improve image quality of accelerated 4D-MRI. Radiother. Oncol. 2021;158:215–223 doi: 10.1016/J.RADONC.2020.12.032. [PubMed: 33412207]
23. Feng L, Axel L, Chandarana H, Block KT, Sodickson DK, Otazo R. XD-GRASP: Golden-angle radial MRI with reconstruction of extra motion-state dimensions using compressed sensing. Magn. Reson. Med. 2016;75:775–788 doi: 10.1002/mrm.25665. [PubMed: 25809847]
24. Paulson ES, Ahunbay E, Chen X, et al. 4D-MRI driven MR-guided online adaptive radiotherapy for abdominal stereotactic body radiation therapy on a high field MR-Linac: Implementation and initial clinical experience. Clin. Transl. Radiat. Oncol. 2020;23:72 doi: 10.1016/J.CTRO.2020.05.002. [PubMed: 32490218]
25. Huttinga NRF, Van Den Berg CAT, Luijten PR, Sbrizzi A. MR-MOTUS: model-based non-rigid motion estimation for MR-guided radiotherapy using a reference image and minimal k-space data. Phys. Med. Biol. 2020;65 doi: 10.1088/1361-6560/AB554A.
26. Freedman JN, Gurney-Champion OJ, Nill S, et al. Rapid 4D-MRI reconstruction using a deep radial convolutional neural network: Dracula. Radiother. Oncol. 2021;159:209–217 doi: 10.1016/J.RADONC.2021.03.034. [PubMed: 33812914]
27. Terpstra ML, Maspero M, D'Agata F, et al. Deep learning-based image reconstruction and motion estimation from undersampled radial k-space for real-time MRI-guided radiotherapy. Phys. Med. Biol. 2020;65 doi: 10.1088/1361-6560/AB9358.
28. Huynh E, Hosny A, Guthier C, et al. Artificial intelligence in radiation oncology. Nat. Rev. Clin. Oncol. 2020;17:771–781 doi: 10.1038/S41571-020-0417-8. [PubMed: 32843739]
29. Feng L, Tyagi N, Otazo R. MRSIGMA: Magnetic Resonance SIGnature MAtching for real-time volumetric imaging. Magn. Reson. Med. 2020;84:1280–1292 doi: 10.1002/MRM.28200. [PubMed: 32086858]
30. Han P, Chen J, Xiao J, et al. Single projection driven real-time multi-contrast (SPIDERM) MR imaging using pre-learned spatial subspace and linear transformation. Phys. Med. Biol. 2022;67 doi: 10.1088/1361-6560/AC783E.
31. Feng L, Wen Q, Huang C, Tong A, Liu F, Chandarana H. GRASP-Pro: imProving GRASP DCE-MRI through self-calibrating subspace-modeling and contrast phase automation. Magn. Reson. Med. 2020;83:94–108 doi: 10.1002/mrm.27903. [PubMed: 31400028]
32. Feng L 4D Golden-Angle Radial MRI at Subsecond Temporal Resolution. NMR Biomed. 2022 doi: 10.1002/NBM.4844.
33. Feng L Golden-Angle Radial MRI: Basics, Advances, and Applications. J. Magn. Reson. Imaging 2022 doi: 10.1002/JMRI.28187.

34. Mukaka MM. A guide to appropriate use of Correlation coefficient in medical research. Malawi Med. J. 2012;24:69. [PubMed: 23638278]

35. Feng L, Huang C, Shanbhogue K, Sodickson DK, Chandarana H, Otazo R. RACER-GRASP: Respiratory-weighted, aortic contrast enhancement-guided and coil-unstreaking golden-angle radial sparse MRI. Magn. Reson. Med. 2018;80:77–89 doi: 10.1002/mrm.27002. [PubMed: 29193260]

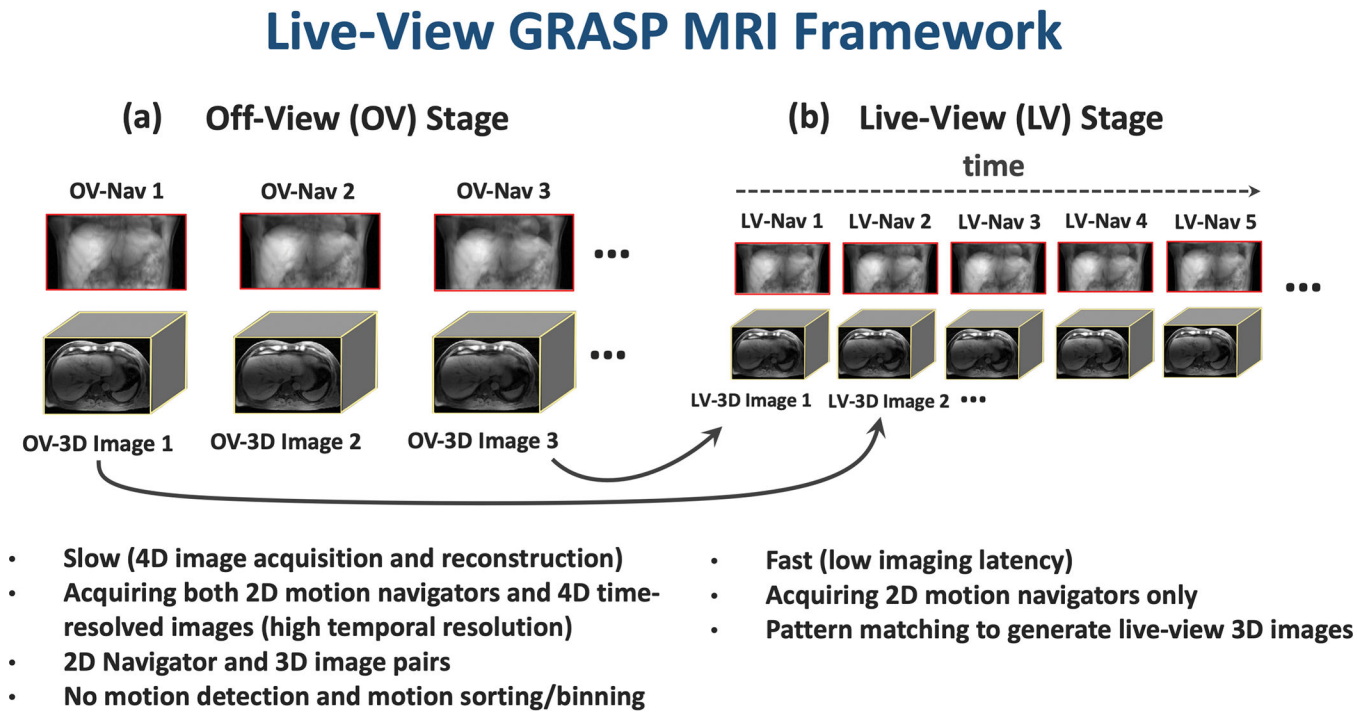

Figure 1.

The live-view GRASP MRI framework includes two imaging stages. The first stage (a) is called an off-view stage that acquires both 3D images and 2D navigators, and each 3D image is linked to a 2D navigator. The second stage (b) is called a live-view stage that only acquires 2D navigators. At each time point, a 2D live-view motion navigator is acquired and is compared to all the 2D off-view motion navigators. A 3D image linked to the off-view motion navigator that best matches the newly acquired live-view navigator is selected as the 3D image for the current time point. In this way, 3D images can be generated efficiently in the live-view stage without lengthy acquisition and reconstruction.

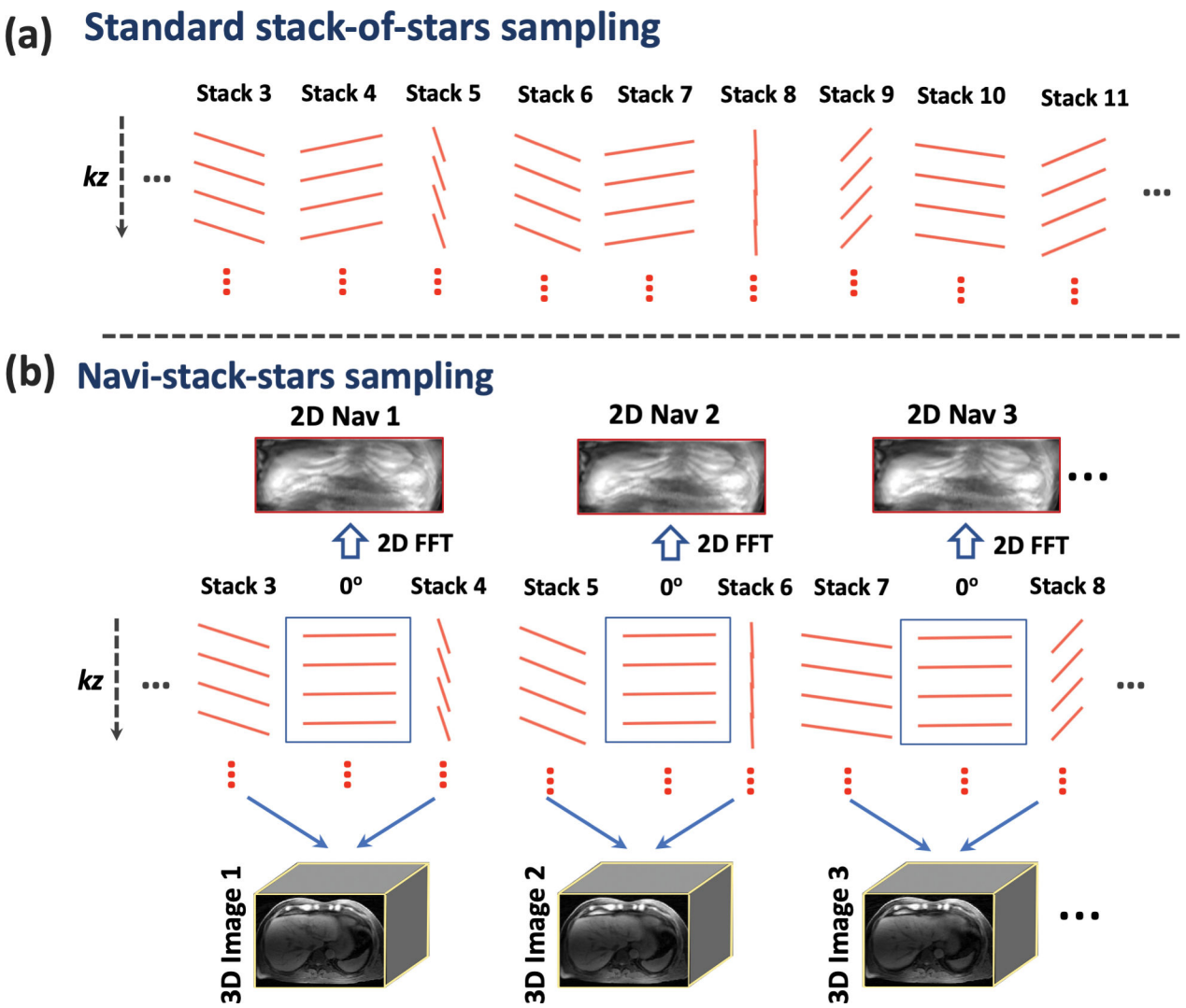

Figure 2.

Comparison of standard stack-of-stars sampling (a) with navi-stack-of-stars sampling (b). Navi-stack-of-stars sampling is modified from the stack-of-stars trajectory, and it alternatively acquires both regular radial stacks rotated by a golden angle and 2D navigator stacks with a 0-degree acquisition angle. A navigator stack is acquired every other two regular radial stacks. From the navigator stacks, coronal 2D projections are obtained with a 2D FFT, and the projections serve as motion navigators. A 3D image is reconstructed from two regular radial stacks (2 radial spokes in each slice), as shown in (b), and the reconstructed 3D image can be linked to a 2D navigator acquired between the two regular stacks.

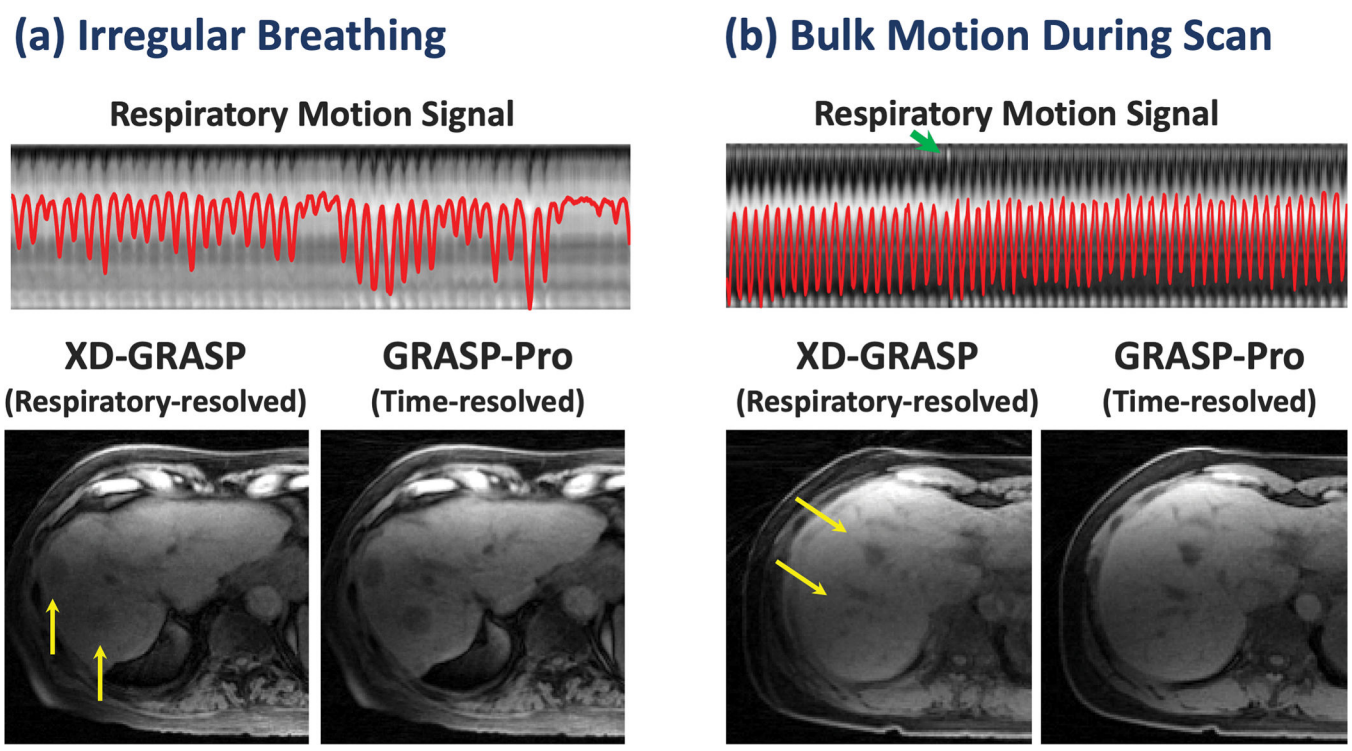

Figure 3.

Comparison of time-resolved high-temporal-resolution 4D images (0.3s per 3D volume) reconstructed using GRASP-Pro with respiratory motion-resolved images (10 respiratory phases) reconstructed using XD-GRASP. (a) In a patient with HCC acquired during irregular breathing, GRASP-Pro reconstruction was able to resolve respiratory motion while XD-GRASP reconstruction suffers from residual motion blurring, particularly in the HCCs (yellow arrows). (b) In a volunteer acquired with body movement during the scan (green arrow), XD-GRASP reconstruction yielded blurring while GRASP-Pro reconstruction enabled better image quality.

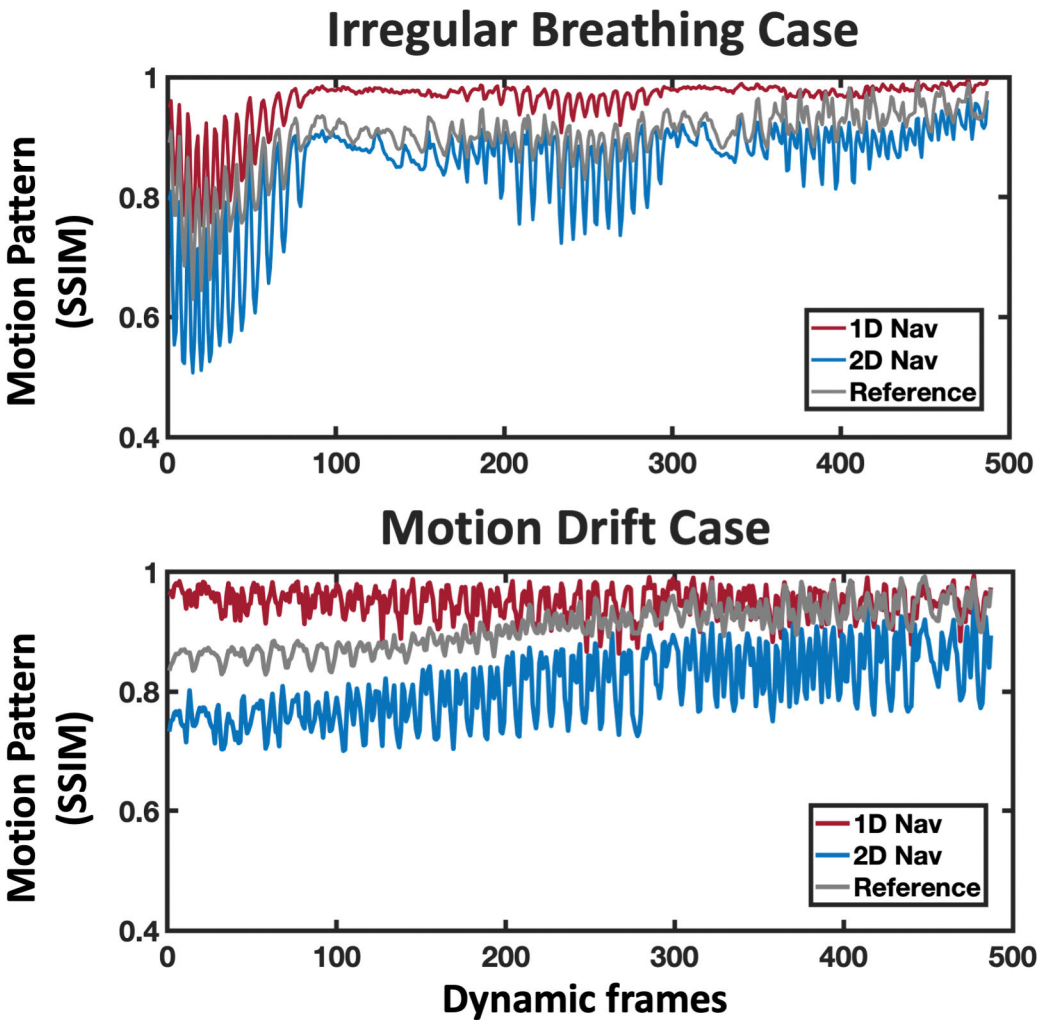

Figure 4.

SSIM curves from two representative subjects from study 1 in experiment 1 (without prescribed breathing instruction during the scans) comparing the performance for detecting respiratory variations using 2D and 1D navigators. Although 2D and 1D navigators could both detect irregular breathing in the first subject, 1D navigators failed to detect a motion drift in the second subject. In contrast, 2D navigators were able to detect the drift as well as the reference 3D images. 1D navigators were obtained by taking the *kz*-directional central k-space lines from the 0° navigator stacks followed by a 1D FFT and multicoil combination using sum of square.

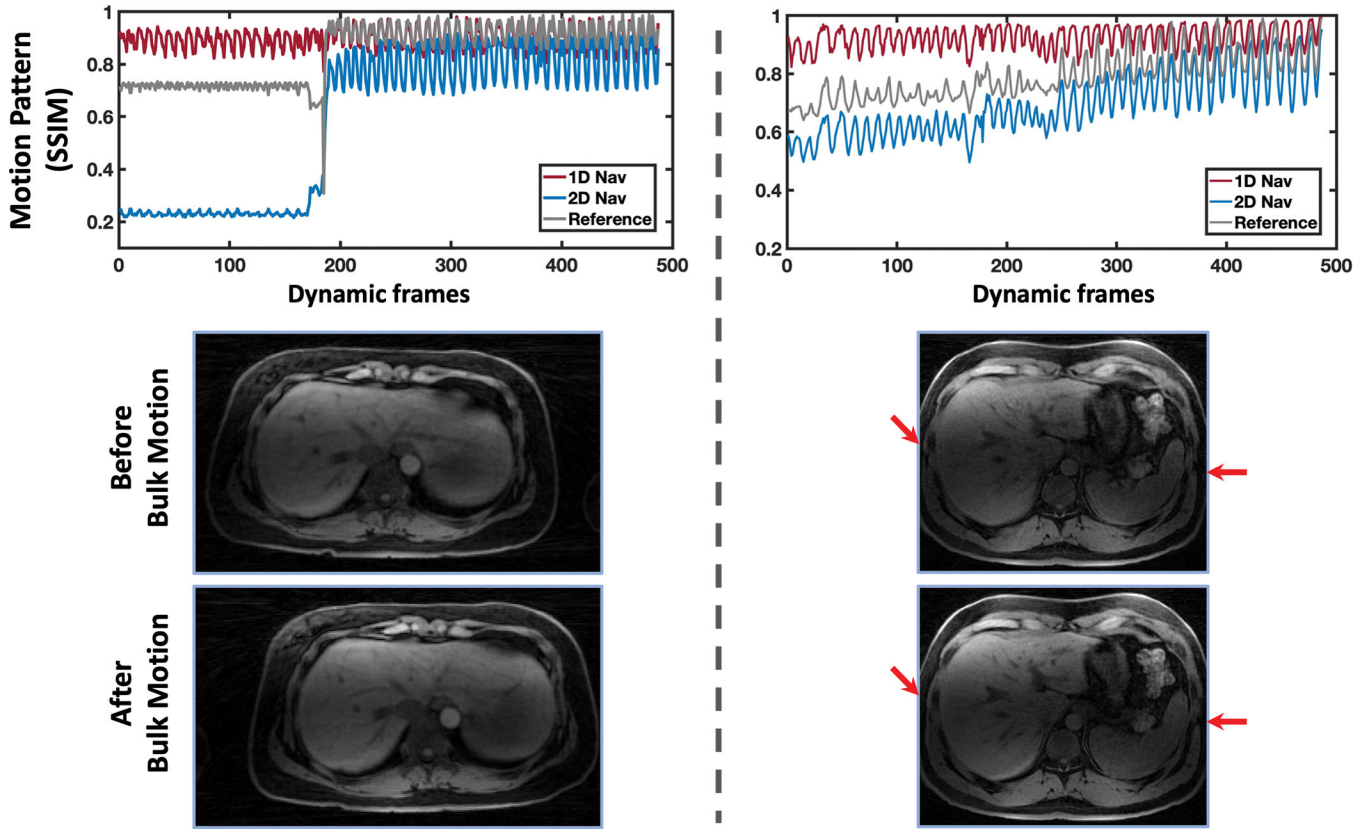

Figure 5.

SSIM curves from two representative subjects from study 2 in experiment 1 (with prescribed body movement during the scans) comparing the performance for detecting respiratory variations using 2D and 1D navigators. The first subject had an obvious body movement while the second subject only had a small movement, as shown in the reference 3D images. For both subjects, 1D navigators failed to detect the body movement, while 2D navigators could successfully detect the motion.

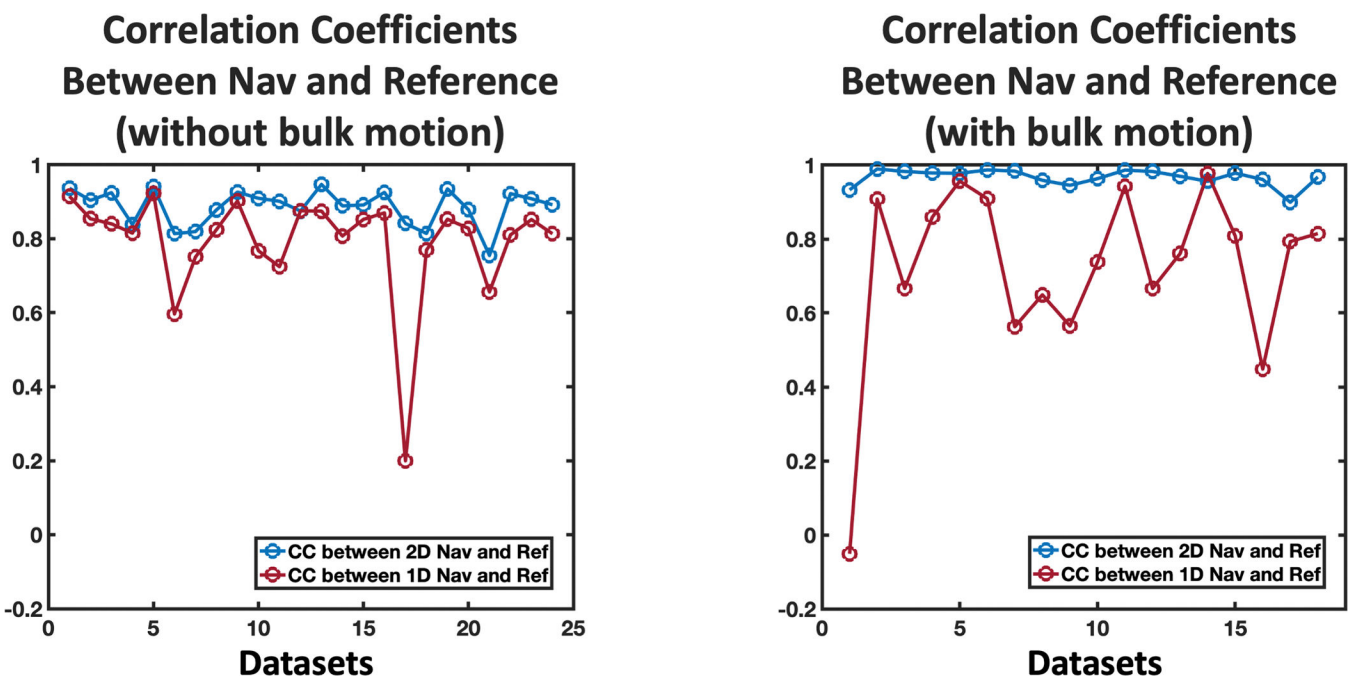

Figure 6.

Correlation coefficients (CCs) for all the 24 datasets from study 1 (left) and all the 18 datasets from study 2 (right) in experiment 1 comparing the SSIM curves between 3D reference images and 2D or 1D navigators. 2D navigators yielded consistent improvement over 1D navigators for detecting respiratory variations and/or body movements in the off-view stage. For study 1, the CCs were 0.886 ± 0.049 between 2D navigators and the reference and were 0.791 ± 0.148 between 1D navigators and the reference. For study 2, the CCs were 0.967 ± 0.023 between 2D navigators and the reference and were 0.721 ± 0.244 between 1D navigators and the reference. A higher CC indicates a higher positive correlation with the reference and thus better performance.

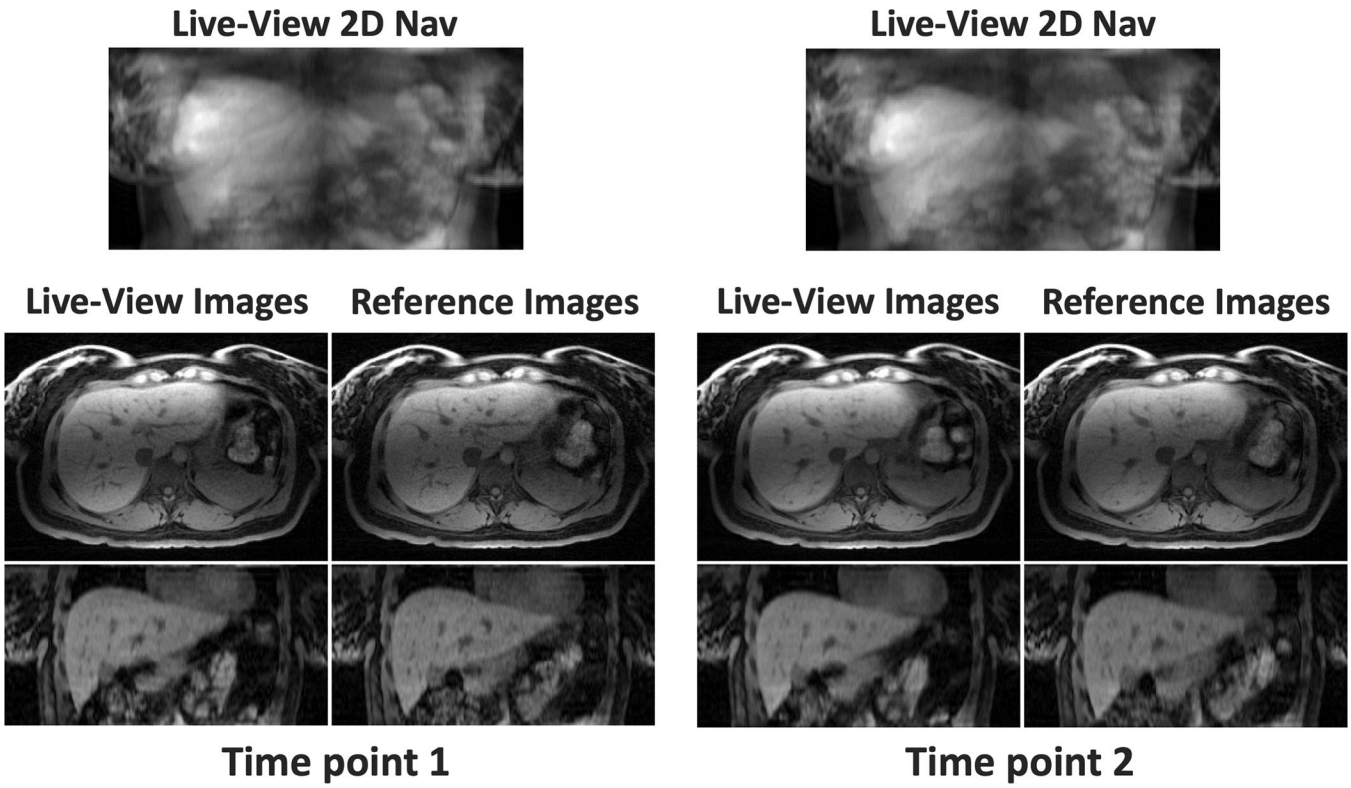

Figure 7.
Two live-view 2D navigators and corresponding live-view 3D images from one subject at two different time points. The live-view 3D images match well with the reference 3D images.

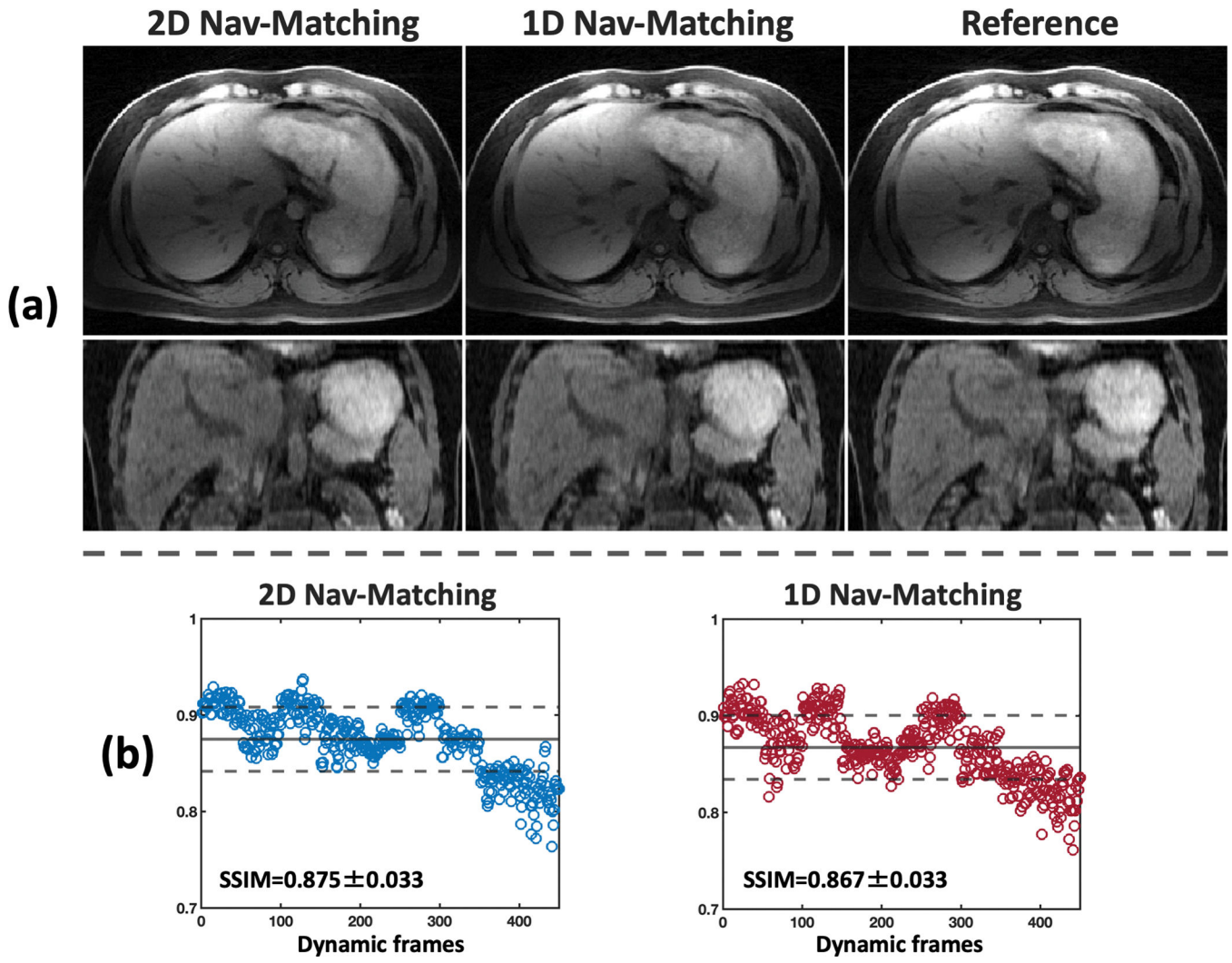

Figure 8.

(a) Comparison of live-view 3D images obtained with 2D nav-matching and 1D nav-matching along with corresponding reference 3D images in one subject. (b) SSIM values between reference 3D images and live-view 3D images with 2D nav-matching (left) and SSIM values between reference 3D images and live-view 3D images with 1D nav-matching (right) from a total of 450 time points (9 subjects and 50 time points each). There were no significant differences in 8 subjects (P=0.074–0.46) between 2D nav-matching and 1D nav-matching, while 2D nav-matching was better (P=0.0039) only in one subject. A higher SSIM indicates better accuracy of nav-matching.

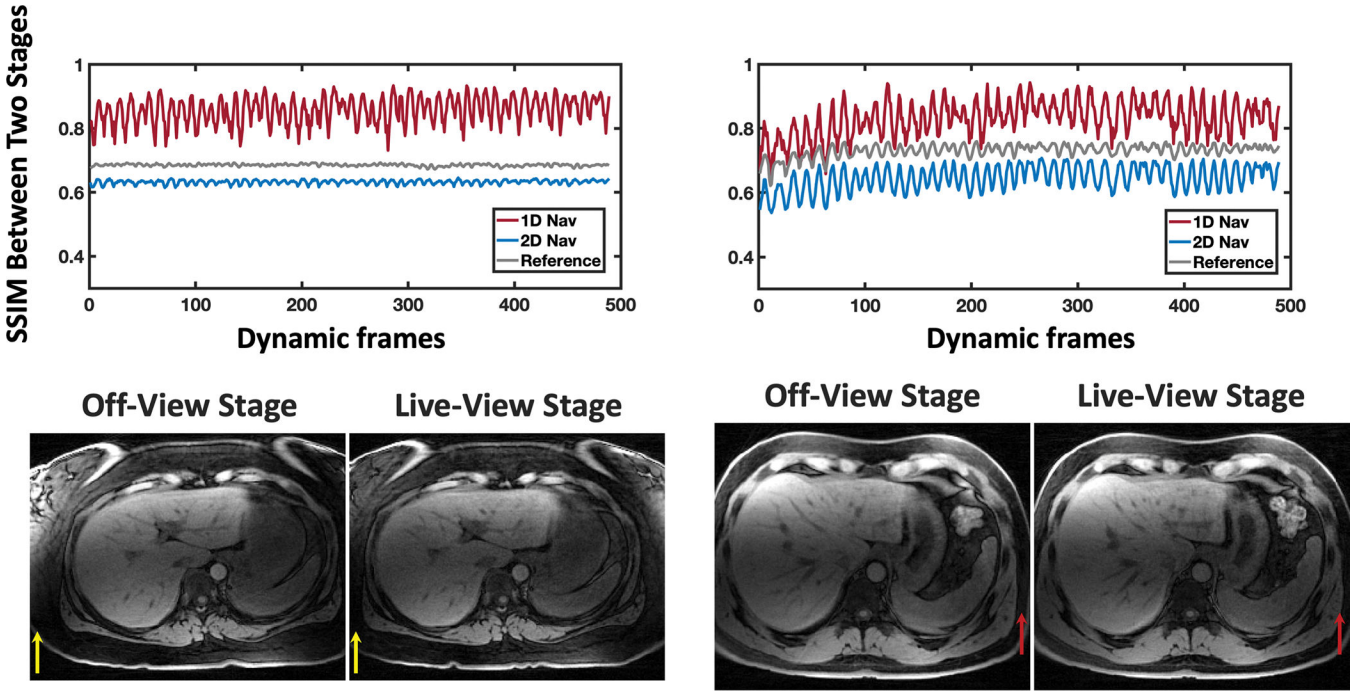

Figure 9.

Comparison of 2D navigators and 1D navigators for detecting body movements that may occur between the off-view and live-view stages. In the first subject (left), there is a clear shift of body position between the off-view stage and the live-view stage (yellow arrows). The SSIM values obtained from both 3D images and 2D navigators are consistently low, indicating successful detection of the movement, while the SSIM values obtained from 1D navigators are higher, suggesting that 1D navigators may not be able to detect the body movement. In the second subject (right), a small shift of body position occurred between the two stages as indicated by the red arrows in the 3D images. The difference of body position could be identified from both 3D images and 2D navigators with consistently low SSIM values, while the SSIM values obtained from 1D navigators are higher.

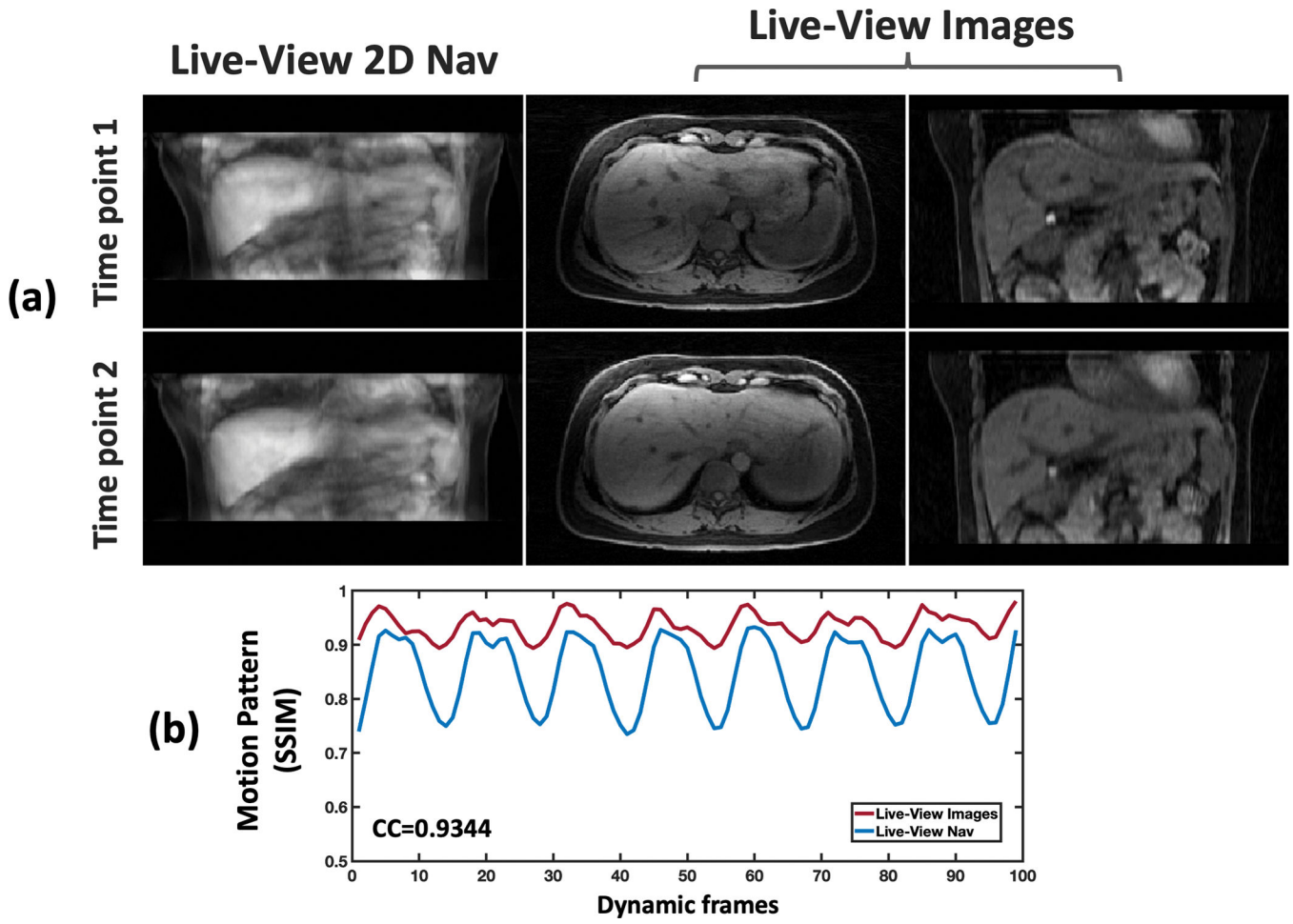

Figure 10.

Live-view 2D navigators and resulting live-view 3D images at two different time points from one subject. SSIM curves calculated from the 3D images (red curve) and the 2D navigators (blue curve) are shown in Figure 10b with a strong correlation (CC=0.9344). A CC above 0.9 indicates a very high positive correlation.